

Dichotomy of heavy and light pairs of holes in the $t - J$ model

A. Bohrdt,^{1, 2,*} E. Demler,³ and F. Grusdt^{4, 5}

¹*ITAMP, Harvard-Smithsonian Center for Astrophysics, Cambridge, MA 02138, USA*

²*Department of Physics, Harvard University, Cambridge, Massachusetts 02138, USA*

³*Institut für Theoretische Physik, ETH Zurich, 8093 Zurich, Switzerland*

⁴*Department of Physics and Arnold Sommerfeld Center for Theoretical Physics (ASC), Ludwig-Maximilians-Universität München, Theresienstr. 37, München D-80333, Germany*

⁵*Munich Center for Quantum Science and Technology (MCQST), Schellingstr. 4, D-80799 München, Germany*

(Dated: October 6, 2022)

A key step in unraveling the mysteries of materials exhibiting unconventional superconductivity is to understand the underlying pairing mechanism. While it is widely agreed upon that the pairing glue in many of these systems originates from antiferromagnetic spin correlations [1–3], a microscopic description of pairs of charge carriers remains lacking. Here we use state-of-the art numerical methods to probe the internal structure and dynamical properties of pairs of charge carriers in quantum antiferromagnets in four-legged cylinders. Exploiting the full momentum resolution in our simulations, we are able to distinguish two qualitatively different types of bound states: a highly mobile, meta-stable pair, which has a dispersion proportional to the hole hopping t , and a heavy pair, which can only move due to spin exchange processes and turns into a flat band in the Ising limit of the model. Understanding the pairing mechanism can on the one hand pave the way to boosting binding energies in related models [4], and on the other hand enable insights into the intricate competition of various phases of matter in strongly correlated electron systems [5, 6].

Introduction.— Following the discovery of high temperature superconductivity in the cuprates, understanding the mechanism by which pairs of charge carriers can form in a system with repulsive interactions has been a key question in the field. Motivated by experimental results on the cuprate materials, a lot of theoretical and numerical work has focused on identifying the potential pairing symmetry [7, 8] as well as the binding energies in these microscopic models [9, 10]. Despite a vast research effort over several decades, the existence of a superconducting phase in the simplest model describing interacting electrons, the Fermi-Hubbard model, remains debated [6]. Competing orders, such as charge density waves and stripes, contribute to the difficulty in realizing as well as understanding superconductivity [5]. In order to unravel the competition between different orders, and thus the conditions for the existence of a superconducting phase, it is essential to gain a deeper understanding of the nature of pairs of charge carriers. The existence of pairs close to half-filling does not imply that for a finite density of holes, the system necessarily realizes a d -wave paired state. Instead, a finite number of charge carriers can for example self-organize into a charge or pair density wave state [11]. However, understanding whether and how pairs form in the two-hole problem is crucial to the subsequent understanding of self-organization of many holes.

Here we approach the question of the underlying binding mechanism from a new perspective: through novel spectroscopic tools, we search for bound states of charge carriers in a quantum antiferromagnet and directly probe their internal structure. In particular, we numerically

simulate rotational two-hole spectra, where different angular momenta can be imparted on the system, using time-dependent matrix product states. Crucially, these rotational spectra go beyond the standard pairing correlations through the momentum resolution they provide. The momentum dependence of the peaks in the spectral function enables direct insights into the effective mass of the pairs, which is an essential property for understanding their ability to condense at finite doping and temperature.

We study pairing between holes doped into the two-dimensional $t - J$ model, which corresponds to the enigmatic Fermi-Hubbard model to second order in t/U (up to next-nearest neighbor hopping terms, where U is the on-site interaction) and describes electrons in cuprates [12]:

$$\hat{\mathcal{H}}_{t-J} = -t \hat{\mathcal{P}} \sum_{\langle i,j \rangle} \sum_{\sigma} \left(\hat{c}_{i,\sigma}^{\dagger} \hat{c}_{j,\sigma} + \text{h.c.} \right) \hat{\mathcal{P}} + J \sum_{\langle i,j \rangle} \hat{\mathbf{S}}_i \cdot \hat{\mathbf{S}}_j - \frac{J}{4} \sum_{\langle i,j \rangle} \hat{n}_i \hat{n}_j, \quad (1)$$

where $\hat{\mathcal{P}}$ projects to the subspace with maximum single occupancy per site; $\hat{\mathbf{S}}_j$ and \hat{n}_j denote the on-site spin and density operators, respectively. In our numerical simulations, we consider a 40 site long, four-legged cylinder.

In order to probe a possible bound state of two charges, we consider an extension of conventional angle-resolved photoemission spectroscopy (ARPES). In particular, we excite the system by creating not one, but two charges while simultaneously imparting angular momentum on the system. The resulting spectra thus directly contain information about the existence of possible bound states, their ground state energy, as well as their dispersion re-

* Corresponding author email: bohrdt@fas.harvard.edu

lation. In our numerical matrix product state calculations, we find well-defined peaks in the rotational spectral function for all angular momenta, for spin singlet as well as triplet pairs, and throughout an extended frequency range.

In order to gain a deeper understanding of the rotational two-hole spectra, we also consider the conceptually simpler $t - J_z$ model, where the $SU(2)$ invariant spin interactions are replaced by Ising type interactions. Without additional spin dynamics, a direct comparison of our numerical results to an effective theory describing pairs of charge carriers bound by strings is possible, yielding excellent agreement in terms of the existence as well as the dispersion of the various bound states we observe. In particular, we discover a strongly dispersive low-energy peak, with a dispersion scaling with the hole hopping t , as well as completely flat bands at competitive energies. We attribute the flat bands to destructive interference of pairs with d -wave symmetry [13].

Upon introducing spin dynamics, the flat bands develop into weakly dispersive bands, whereas the t -dependent feature remains largely unchanged. We thus discover two qualitatively different kinds of bound states: highly dispersive peaks, including a high energy feature with strong spectral weight in the s -wave spectra; and a weakly dispersive band, which has a high amount of spectral weight in the d -wave spectra. The dispersion of the latter is determined by the spin coupling J . The emergence of a slow time-scale set by J is intuitive in the case of a single hole, which forms a spinon-holon bound state and can thus only move as fast as the spin excitation [14]. In contrast, it is surprising to find a bound state of two holes, which in principle can individually move with a hopping amplitude t , but when bound into a pair have a dispersion given by the spin exchange.

The remainder of this paper is organized as follows. We start by introducing the rotational two-hole spectra. We then discuss results for the $t - J_z$ model, where the $SU(2)$ invariant spin interactions are replaced by Ising-type interactions. We discuss the features found in the numerically obtained spectra in detail and compare to a semi-analytical theoretical description of pairs of charge carriers [15]. Finally, we consider the full $t - J$ model.

Rotational Spectra.— In order to probe the internal structure of pairs of charge carriers, we study rotational spectra. We define an operator $\hat{\Delta}_{m_4}(\mathbf{j}, \sigma, \sigma')$ that creates a pair of holes on the bonds adjacent to site \mathbf{j} with discrete C_4 angular momentum $m_4 = 0, 1, 2, 3$ as

$$\hat{\Delta}_{m_4}(\mathbf{j}, \sigma, \sigma') = \sum_{\mathbf{i}: \langle \mathbf{i}, \mathbf{j} \rangle} e^{i \frac{\pi}{2} m_4 \varphi_{\mathbf{i}-\mathbf{j}}} \hat{c}_{\mathbf{i}, \sigma'} \hat{c}_{\mathbf{j}, \sigma}, \quad (2)$$

with $\varphi_{\mathbf{r}} = \arg(\mathbf{r})$ the polar angle of \mathbf{r} . In order to annihilate a spin-singlet, we define the singlet pair operator (and similar for triplets) as

$$\hat{\Delta}_{m_4}^{(s)}(\mathbf{j}) = \hat{\Delta}_{m_4}(\mathbf{j}, \uparrow, \downarrow) - \hat{\Delta}_{m_4}(\mathbf{j}, \downarrow, \uparrow). \quad (3)$$

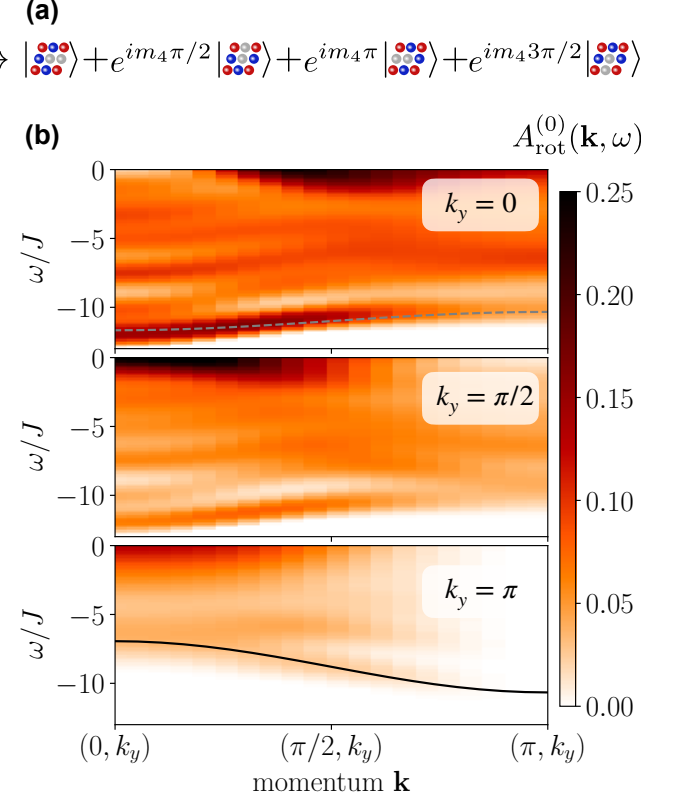


FIG. 1. **Rotational spectroscopy of two holes** in a singlet state in the $t - J$ model with $t/J = 3$, on a 40×4 cylinder, based on a time evolution up to $T_{max}/J = 3$ and bond dimension $\chi = 1200$. (a) Sketch of the response probed by the rotational spectrum. (b) The upper, middle, and lower plots correspond to $k_y = 0, \pi/2, \pi$ and data is shown as a function of momentum k_x and frequency ω/J for $m_4 = 0$; $m_4 = 2$ exhibits similar features, see [13]. Gray dashed lines correspond to a cosine dispersion $-2J\alpha \cos(k_x) + b_J$, black line corresponds to a cosine dispersion $-2t\alpha \cos(k_x) + b_t$, where $\alpha = 0.33$ in both cases, $b_J = -11$, and $b_t = -9$.

The simplest term creating a spin-singlet excitation with discrete angular momentum m_4 , charge two, and total momentum \mathbf{k} is directly given by the spatial Fourier transform of the singlet pair operator as

$$\hat{\Delta}_{m_4}^{(s)}(\mathbf{k}) = \sum_{\mathbf{j}} \frac{e^{-i\mathbf{k}\cdot\mathbf{j}}}{\sqrt{V}} \hat{\Delta}_{m_4}^{(s)}(\mathbf{j}) \quad (4)$$

with volume V . The discrete angular momentum m_4 is a good quantum number at C_4 invariant momenta $\mathbf{k} = (0, 0), (\pi, \pi)$ only. Based on this operator, we now consider the rotational Green's function

$$\mathcal{G}_{\text{rot}}^{(m_4)}(\mathbf{k}, t) = \theta(t) \langle \Psi_0 | \hat{\Delta}_{m_4}^{(s)\dagger}(\mathbf{k}, t) \hat{\Delta}_{m_4}^{(s)}(\mathbf{k}, 0) | \Psi_0 \rangle, \quad (5)$$

which we calculate using time-dependent matrix product states [16–18]. The corresponding two-hole rotational spectrum, $-\pi^{-1} \text{Im} \mathcal{G}_{\text{rot}}^{(m_4)}(\mathbf{k}, \omega)$, in Lehmann representa-

tion is

$$A_{\text{rot}}^{(m_4)}(\mathbf{k}, \omega) = \sum_n \delta(\omega - E_n + E_0^0) |\langle \Psi_n | \hat{\Delta}_{m_4}^{(s)}(\mathbf{k}) | \Psi_0^0 \rangle|^2, \quad (6)$$

where $|\Psi_0^0\rangle$ (E_0^0) is the ground state (energy) of the undoped system and $|\Psi_n\rangle$ (E_n) are the eigenstates (eigenenergies) with two holes.

The two-hole rotational spectral function defined above is closely related to the dynamical pairing correlations frequently considered in the literature [6, 19, 20],

$$P(\omega) = \int dt e^{i\omega t} \langle \hat{\Delta}_{m_4}^{(s)\dagger}(t) \hat{\Delta}_{m_4}^{(s)}(0) \rangle, \quad (7)$$

where $\hat{\Delta}_{m_4}^{(s)} = \sum_j \hat{\Delta}_{m_4}^{(s)}(\mathbf{j})$. We, however, consider the full momentum dependence of the pairing correlations, which enables direct insights into the center-of-mass dispersion of pairs of charge carriers.

The resulting rotational spectra thus directly probe the existence of bound states and their internal structure: If a bound state of two holes with long-lived rotational excitations exists, the rotational spectra should exhibit well-defined coherent peaks. If on the other hand such bound states do not exist, the excitation with the rotational operator $\hat{\Delta}_{m_4}(\mathbf{k})$ will lead to a broad continuum in the corresponding spectral function.

In Fig. 1, we show the two-hole spectral function without additional angular momentum, i.e. $m_4 = 0$ (*s*-wave), for the $t - J$ model for momenta $k_y = 0, \pi/2$, and π and $0 \leq k_x \leq \pi$. We find a well-defined coherent peak at low energies for all momenta, indicating the existence of a bound state. The spectrum furthermore reveals a plethora of different features, including a highly dispersive band (black line) as well as bands with a dispersion proportional to the spin-exchange J (gray dashed lines). At momentum $\mathbf{k} = (\pi, \pi)$, the spectral weight vanishes for all energies since $\hat{\Delta}_0^{(s)}(\mathbf{k} = (\pi, \pi)) = 0$.

In order to gain a deeper understanding of these intriguing results, we take a step back and analyze the conceptually simpler $t - J_z$ model in the following section.

The $t - \text{XXZ}$ model.— We now consider a modification of the $t - J$ model, where the SU(2) invariant spin interactions are replaced by in-plane and Ising-type spin interactions with coupling constants J_\perp and J_z :

$$\hat{\mathcal{H}}_{t-\text{XXZ}} = \sum_{\langle \mathbf{i}, \mathbf{j} \rangle} \left(J_\perp \left(\hat{S}_\mathbf{i}^x \hat{S}_\mathbf{j}^x + \hat{S}_\mathbf{i}^y \hat{S}_\mathbf{j}^y \right) + J_z \hat{S}_\mathbf{i}^z \hat{S}_\mathbf{j}^z \right) - t \hat{\mathcal{P}} \sum_{\langle \mathbf{i}, \mathbf{j} \rangle} \sum_{\sigma} \left(\hat{c}_{\mathbf{i}, \sigma}^\dagger \hat{c}_{\mathbf{j}, \sigma} + \text{h.c.} \right) \hat{\mathcal{P}} - \frac{J_z}{4} \sum_{\langle \mathbf{i}, \mathbf{j} \rangle} \hat{n}_\mathbf{i} \hat{n}_\mathbf{j}. \quad (8)$$

In the limit of $J_\perp \ll J_z$, also called the $t - J_z$ model, the lack of spin dynamics facilitates our theoretical understanding. Experimentally, the anisotropic interactions can for example be realized by employing Rydberg interactions [21].

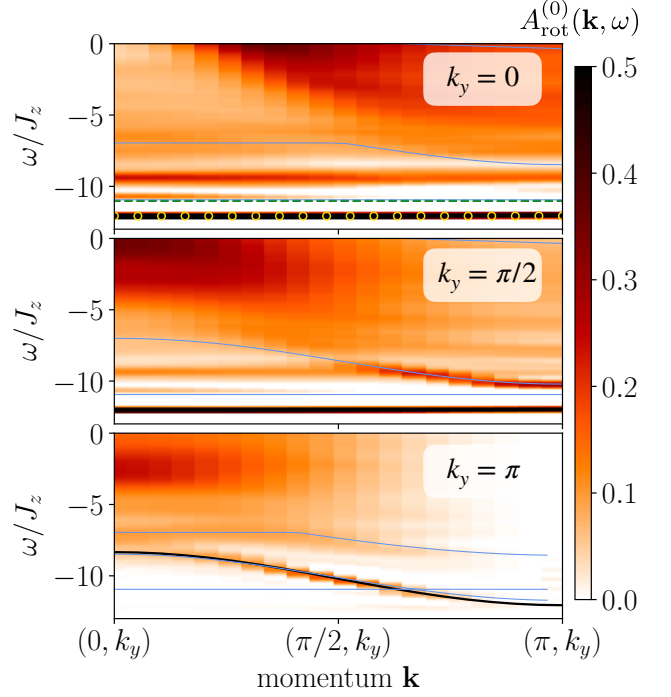


FIG. 2. **Two hole rotational spectra in the $t - \text{XXZ}$ model** for $t/J_z = 3$ and $J_\perp/J_z = 0.1$ and $m_4 = 0$ (*s*-wave) on a 40×4 cylinder, based on time evolution up to $T_{\text{max}}/J_z = 10$ and bond dimension $\chi = 600$. The colormap corresponds to numerical matrix product state simulations of the singlet two-hole rotational spectrum, blue lines are geometric string theory predictions for the position of states (all shifted by $-0.35J$), and the black line is a cosine fit. The upper, middle, and lower plots correspond to $k_y = 0, \pi/2, \pi$ and data is shown as a function of momentum k_x and frequency ω/J_z . The overall ground state energy for two holes is marked by orange circles for $k_y = 0$, and the green dashed line in the top panel corresponds to twice the energy of a single hole.

Remarkably, the two-hole spectral function, Fig. 2, exhibits a highly dispersive peak with a mass proportional to $1/t$; I.e., we find a long-lived, tightly bound state of two holes, which can move as fast as the hole hopping t . This is in stark contrast to the case of a single hole in the same model, which has a very high effective mass $\gg 1/t$ and thus an almost flat dispersion [22], since it can only move due to Trugman loops [23], which are higher order processes.

In Fig. 3, we further analyze the scaling of the mass of the pair by analyzing the position ω_{max} of the lowest energy peak at $k_y = \pi$ as a function of k_x for different values of $t/J_z = 1, 2, 3$ and $J_\perp/J_z = 0.1$. Note that here, the frequency ω_{max} is shown in units of the hole hopping t . We added a constant to the curves for different values of t/J_z to show the remarkable agreement in the overall shape of the dispersive peak for different values of t/J_z , thus highlighting the scaling with the hole hopping t .

The lowest lying peak for $k_y = 0$ and $k_y = \pi/2$ is – within our numerical resolution – completely flat. Note

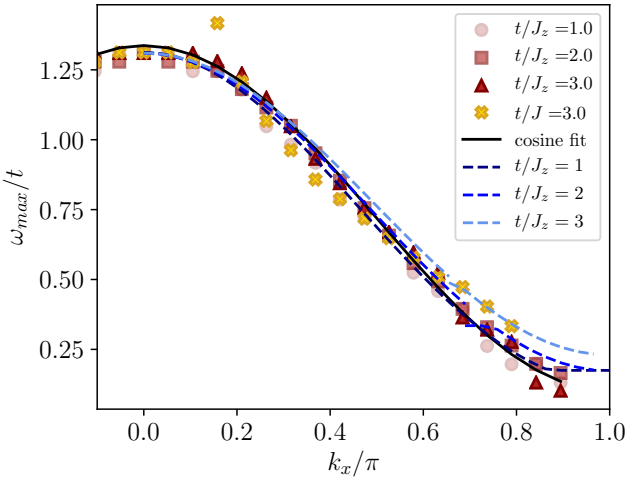


FIG. 3. **Strongly dispersive pair state** in the t –XXZ model for $t/J_z = 1, 2, 3$ and $J_{\perp}/J_z = 0.1, 1.0$ and $m_4 = 0$ (*s*-wave). The symbols correspond to the position of the lowest energy peak at $k_y = \pi$ extracted from numerical matrix product state simulations of the singlet two-hole rotational spectrum. Yellow crosses correspond to the isotropic case, $J_z = J_{\perp} = J$ with $t/J = 3$. All data points are shifted vertically to collapse at $k_x = 0$. Blue dashed lines are geometric string theory predictions for the position of the lowest states. For $t/J_z = 2, 3$, the lowest two states predicted by the geometric string theory are shown. Black line is a cosine fit, $0.62 \cos(k_x) + 0.72$, to the extracted peak positions for $t/J_z = 3$, $J_{\perp}/J_z = 0.1$.

that the situation of two unbound, and thus approximately immobile, holes should have a very small matrix element in the spectral function considered here, and therefore cannot account for the pronounced flat band peaks we find in the two-hole spectra. This is further corroborated by the direct comparison of the energy for two holes ($E_{2h} - E_{0h} = -12.08J_z$, orange circles in top panel Fig. 2) and twice the energy of a single hole ($2 \cdot (E_{1h} - E_{0h}) = -11.01J_z$, green dashed line in top panel Fig. 2).

In a companion paper [15], we extend the geometric string theory developed for a single hole [22, 24] to the case of two charge carriers. In particular, this geometric string theory approach describes the properties of two holes bound together by a string of displaced spins, and thus provides estimates of the energy and dispersion relation of such pair states, see blue lines in Figs. 2 and 3. Note that the existence of a state at a given energy does not imply that said state is visible in the spectral function, since the spectral weight, i.e. the overlap with the excitation we consider, can still be zero.

The geometric string theory correctly predicts the highly dispersive peak, as well as the existence of completely flat bands. The latter have also been predicted by a related theoretical study [25].

Results for the t – J model.— In the isotropic case,

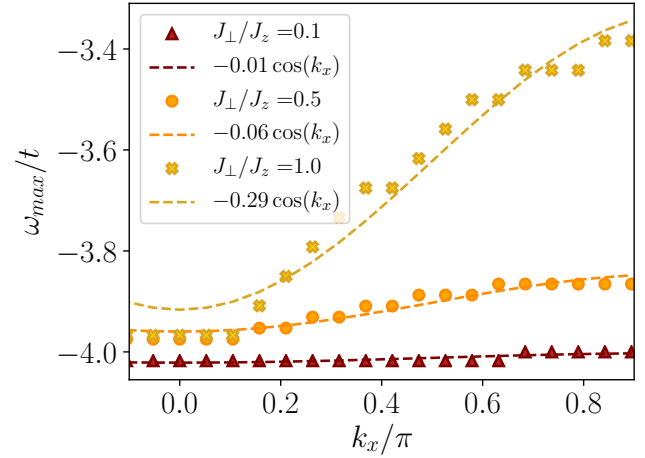


FIG. 4. **Weakly dispersive pair** in the t –XXZ model for $t/J_z = 3$, $J_{\perp}/J_z = 0.1, 0.5, 1.0$, and $m_4 = 2$ (*d*-wave). The symbols correspond to the position of the lowest energy peak at $k_y = 0$ extracted from matrix product state simulations of the singlet two-hole rotational spectrum. Dashed lines are a cosine fit to the extracted peak positions with prefactor as indicated in the legend, and an additional offset (not indicated).

$J_{\perp} = J_z$, the strongly dispersive peak remains visible, see Fig. 1 bottom. In Fig. 3, we compare the peak position for the isotropic t – J model with the t –XXZ model with $J_{\perp}/J_z = 0.1$ and find that the momentum dependence along the x -direction of the lowest lying peak for $k_y = \pi$ is qualitatively very similar between the two cases. This indicates in particular that also in the t – J model, a highly mobile, tightly bound pair state exists.

The flat bands, particularly visible in the $J_{\perp}/J_z = 0.1$ case at momenta $k_y = 0, \pi/2$, acquire a dispersion approximately proportional to J_{\perp}^2/J_z , as can be seen in the top and middle plot in Fig. 1. We analyze this behavior in more detail by explicitly extracting the peak position ω_{\max} at $k_y = 0$ for $t/J_z = 3$ and different values of J_{\perp}/J_z in Fig. 4.

Again, the geometric string theory [15] correctly captures the highly dispersive peak with mass proportional to $1/t$ (black lines) discussed in Fig. 3. However, since this theoretical description does not account for spin dynamics, it does not predict the dispersion proportional to J_{\perp}^2/J_z (gray dashed lines). The corresponding bands in the t – J_z model are flat, as predicted by the geometric string theory.

Different angular momenta.— Thus far, we considered the case of *s*-wave pairs, i.e. $m_4 = 0$ and found a well-defined coherent peak at low energies. In Fig. 5, we show the spectral function for the t – J model at $t/J = 3$ at momentum $k_y = 0$ for $m_4 = 0, 2$, corresponding to *s*- and *d*-wave excitations. Note, however, that the 40×4 cylinder geometry used in our numerical simulations breaks the C_4 symmetry, and therefore $m_4 = 0$ and $m_4 = 2$ excitations can hybridize.

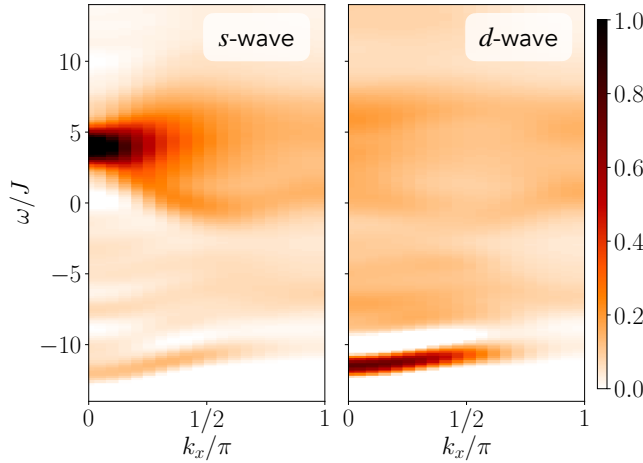


FIG. 5. **Angular momentum dependence** of the rotational two-hole spectra in the $t - J$ model with $t/J = 3$ for $m_4 = 0, 2$ (left, right column) and $k_y = 0$, obtained from time-dependent matrix product state simulations of the singlet two-hole rotational spectrum.

The spectral weight exhibits a strong dependence on the excitation, see Fig. 5. Before, we have identified two qualitatively different types of bound states: a strongly dispersive band, see Fig. 3, and a weakly dispersive band, see Fig. 4. By considering different rotational excitations, we find that the weakly dispersive pair, realizing the overall ground state, has most spectral weight for the d -wave ($m_4 = 2$) excitation, whereas for the s -wave ($m_4 = 0$) excitation, a large fraction of the spectral weight appears in a strongly dispersive high energy feature. This high-energy feature is also predicted by the geometric string theory [15].

The hybridization of different m_4 excitations in the cylinder geometry leads to the appearance of the weakly dispersive feature, found with strong spectral weight for $m_4 = 2$, also at $m_4 = 0$, albeit with a smaller spectral weight. The overall lowest energy peak appears at momentum $\mathbf{k} = (0, 0)$ and $m_4 = 0, 2$.

We note that in early exact diagonalization studies on small systems [19, 20], the integration over all momenta, or the consideration of only momentum zero, leads to a much sharper low energy peak in the d -wave than in the s -wave case. We attribute this to the widely different dispersions of the s - and d -wave peaks revealed here, and the exact C_4 symmetry in small systems.

The geometric string theory correctly predicts the d -wave character of the weakly dispersive band, as well as the accumulation of spectral weight at $\mathbf{k} = (0, 0)$ [15]. A more detailed comparison of spectral weights for different values of m_4 shows good qualitative agreement at low energies (see supplementary material).

So far, we considered a singlet excitation. In order to annihilate a triplet instead, we define the triplet pair operator as

$$\hat{\Delta}_{m_4}^{(t)}(\mathbf{j}) = \hat{\Delta}_{m_4}(\mathbf{j}, \uparrow, \downarrow) + \hat{\Delta}_{m_4}(\mathbf{j}, \downarrow, \uparrow). \quad (9)$$

Upon considering the corresponding triplet spectral function, we find that the lowest lying peaks are at higher energies than in the case of the singlet spectral function. This finding furthermore suggests that the lowest energy peak in the singlet spectral function cannot be attributed to unbound states of two holes.

Summary and Outlook.— In this work, we extensively studied the properties of pairs of charge carriers in the $t - J$ and $t - \text{XXZ}$ model through rotational spectra. We find well defined coherent peaks at low energies for all momenta and angular momenta m_4 . Our work provides the first extensive numerical study of the mass of pairs of charge carriers in extended systems. We have revealed two qualitatively different types of bound states: First, a weakly dispersive peak with a dispersion approximately proportional to J_\perp^2/J_z , which has most spectral weight for a d -wave excitation. And second, a highly dispersive peak, which corresponds to tightly bound pairs with a mass proportional to $1/t$. We find the same signatures of these light pairs of charge carriers in the $t - J_z$ and the SU(2) invariant $t - J$ models. The band corresponding to these light pairs, as well as the bands corresponding to heavy pairs, are qualitatively captured by a semi-analytic geometric string theory approach [15].

An intriguing direction for future research is the direct experimental probe of the two-hole rotational states. Understanding the pairing mechanism in the Fermi-Hubbard and related models has been one of the key motivations in the development of quantum simulators, and in particular cold atoms in optical lattices [26]. In the past two decades, remarkable progress has been made in the field [27, 28], and several proposals to probe the pairing symmetry have been put forward [29, 30]. More recently, the single-hole spectral function has been measured experimentally [31, 32]. Using additional lattice modulations, the two-hole rotational spectral function considered here could be accessed experimentally. In solid state experiments, the s -wave two-hole spectral function can be accessed through coincidence angle-resolved photo-emission spectroscopy [33], which relies on simultaneous measurements of two photo-electrons and provides direct insights into the pair Green's function. A different approach is based on Anderson-Goldman pair tunneling in a tunnel junction setup [34–36]: to study the structure of individual pairs in a strongly under-doped quasi-2D material as considered here, we propose to tunnel-couple the latter to a probe-superconductor along z -direction. Momentum resolution can in this case be obtained through an in-plane magnetic field.

The observation of light as well as heavy pairs in the spectra shown here furthermore suggests a real-space and -time experiment. Upon slowly releasing two holes next to each other in a cold atom experiment, a low energy state of the pair can be prepared. In the ensuing time evolution, we predict the pairs to spread through the system in two distinct wave-fronts, corresponding to the light and the heavy pair, respectively.

Finally, the existence of flat or weakly dispersive bands opens a new avenue to understand the many competing orders found experimentally in cuprate materials as well as numerically in Fermi-Hubbard and $t - J$ models at finite doping [6, 37, 38]. In a next step, we will investigate the dichotomy between two types of light and heavy pairs in the Fermi-Hubbard model.

Acknowledgements.— We thank Immanuel Bloch, Antoine Georges, Markus Greiner, Mohammad Hafezi, Lukas Homeier, and Ulrich Schollwöck for fruitful discussions. This research was funded by the Deutsche Forschungsgemeinschaft (DFG, German Research Foundation) under Germany’s Excellence Strategy – EXC-2111 – 390814868, by the European Research Council (ERC) under the European Union’s Horizon 2020 research and innovation programm (Grant Agreement no 948141) — ERC Starting Grant SimUcQuam, by the ARO (grant number W911NF-20-1-0163), and by the NSF through a grant for the Institute for Theoretical Atomic, Molecular, and Optical Physics at Harvard University and the Smithsonian Astrophysical Observatory.

REFERENCES

- [1] D. J. Scalapino. Superconductivity and spin fluctuations. *Journal of Low Temperature Physics*, 117(3):179–188, 1999.
- [2] Toru Moriya and Kazuo Ueda. Antiferromagnetic spin fluctuation and superconductivity. *Reports on Progress in Physics*, 66(8):1299–1341, jul 2003.
- [3] Shane M. O’Mahony, Wangping Ren, Weijiong Chen, Yi Xue Chong, Xiaolong Liu, H. Eisaki, S. Uchida, M. H. Hamidian, and J. C. Séamus Davis. On the electron pairing mechanism of copper-oxide high temperature superconductivity. *Proceedings of the National Academy of Sciences*, 119(37):e2207449119, 2022.
- [4] Annabelle Bohrdt, Lukas Homeier, Immanuel Bloch, Eugene Demler, and Fabian Grusdt. Strong pairing in mixed-dimensional bilayer antiferromagnetic mott insulators. *Nature Physics*, 18(6):651–656, 2022.
- [5] D. J. Scalapino. A common thread: The pairing interaction for unconventional superconductors. *Rev. Mod. Phys.*, 84:1383–1417, Oct 2012.
- [6] Mingpu Qin, Chia-Min Chung, Hao Shi, Ettore Vitali, Claudius Hubig, Ulrich Schollwöck, Steven R. White, and Shiwei Zhang. Absence of superconductivity in the pure two-dimensional hubbard model. *Phys. Rev. X*, 10:031016, Jul 2020.
- [7] D.J. Scalapino. The case for $dx_2 - y_2$ pairing in the cuprate superconductors. *Physics Reports*, 250(6):329–365, 1995.
- [8] C. C. Tsuei and J. R. Kirtley. Pairing symmetry in cuprate superconductors. *Rev. Mod. Phys.*, 72:969–1016, Oct 2000.
- [9] A. L. Chernyshev, P. W. Leung, and R. J. Gooding. Comprehensive numerical and analytical study of two holes doped into the two-dimensional $t - j$ model. *Phys. Rev. B*, 58:13594–13613, Nov 1998.
- [10] P. W. Leung. Low-energy states with different symmetries in the t - j model with two holes on a 32-site lattice. *Phys. Rev. B*, 65:205101, Apr 2002.
- [11] Eduardo Fradkin, Steven A. Kivelson, and John M. Tranquada. Colloquium: Theory of intertwined orders in high temperature superconductors. *Rev. Mod. Phys.*, 87:457–482, May 2015.
- [12] F. C. Zhang and T. M. Rice. Effective hamiltonian for the superconducting cu oxides. *Phys. Rev. B*, 37:3759–3761, Mar 1988.
- [13] See supplementary online material.
- [14] A. Bohrdt, F. Grusdt, and M. Knap. Dynamical formation of a magnetic polaron in a two-dimensional quantum antiferromagnet. *New Journal of Physics*, 22(12):123023, dec 2020.
- [15] F. Grusdt, E. Demler, and A. Bohrdt. Pairing of holes by confining strings in antiferromagnets. *arXiv2207.XXX*, Jul 2022.
- [16] Jonas A. Kjäll, Michael P. Zaletel, Roger S. K. Mong, Jens H. Bardarson, and Frank Pollmann. Phase diagram of the anisotropic spin-2 xxz model: Infinite-system density matrix renormalization group study. *Phys. Rev. B*, 87:235106, Jun 2013.
- [17] Michael P. Zaletel, Roger S. K. Mong, Christoph Karrasch, Joel E. Moore, and Frank Pollmann. Time-evolving a matrix product state with long-ranged interactions. *Phys. Rev. B*, 91:165112, Apr 2015.
- [18] Sebastian Paeckel, Thomas Köhler, Andreas Swoboda, Salvatore R. Manmana, Ulrich Schollwöck, and Claudius Hubig. Time-evolution methods for matrix-product states. *Annals of Physics*, 411:167998, Dec 2019.
- [19] Elbio Dagotto, Jose Riera, and A. P. Young. Dynamical pair susceptibilities in the t - j and hubbard models. *Phys. Rev. B*, 42:2347–2352, Aug 1990.
- [20] Didier Poilblanc, José Riera, and Elbio Dagotto. d-wave bound state of holes in an antiferromagnet. *Phys. Rev. B*, 49:12318–12321, May 1994.
- [21] Elmer Guardado-Sánchez, Benjamin M. Spar, Peter Schauss, Ron Belyansky, Jeremy T. Young, Przemysław Bienias, Alexey V. Gorshkov, Thomas Iadecola, and Waseem S. Bakr. Quench dynamics of a fermi gas with strong nonlocal interactions. *Phys. Rev. X*, 11:021036, May 2021.
- [22] F. Grusdt, M. Kádasz-Nagy, A. Bohrdt, C. S. Chiu, G. Ji, M. Greiner, D. Greif, and E. Demler. Parton theory of magnetic polarons: Mesonic resonances and signatures in dynamics. *Phys. Rev. X*, 8:011046, Mar 2018.
- [23] S. A. Trugman. Interaction of holes in a hubbard antiferromagnet and high-temperature superconductivity. *Phys. Rev. B*, 37:1597–1603, Feb 1988.
- [24] Fabian Grusdt, Annabelle Bohrdt, and Eugene Demler. Microscopic spinon-chargon theory of magnetic polarons in the t - j model. *Phys. Rev. B*, 99:224422, Jun 2019.
- [25] Boris I. Shraiman and Eric D. Siggia. Two-Particle Excitations in Antiferromagnetic Insulators. *Physical Review Letters*, 60(8):740–743, 1988.
- [26] W. Hofstetter, J. I. Cirac, P. Zoller, E. Demler, and M. D. Lukin. High-temperature superfluidity of fermionic atoms in optical lattices. *Phys. Rev. Lett.*, 89:220407, Nov 2002.
- [27] Leticia Tarruell and Laurent Sanchez-Palencia. Quantum simulation of the hubbard model with ultracold fermions in optical lattices. *Comptes Rendus Physique*, 19(6):365 – 393, 2018.

- [28] Annabelle Bohrdt, Lukas Homeier, Christian Reinmoser, Eugene Demler, and Fabian Grusdt. Exploration of doped quantum magnets with ultracold atoms. *Annals of Physics*, 435:168651, 2021. Special issue on Philip W. Anderson.
- [29] A. M. Rey, R. Sensarma, S. Fölling, M. Greiner, E. Demler, and M. D. Lukin. Controlled preparation and detection of d-wave superfluidity in two-dimensional optical superlattices. *EPL (Europhysics Letters)*, 87(6):60001–, 2009.
- [30] Takuya Kitagawa, Alain Aspect, Markus Greiner, and Eugene Demler. Phase-sensitive measurements of order parameters for ultracold atoms through two-particle interferometry. *Phys. Rev. Lett.*, 106:115302, Mar 2011.
- [31] Peter T. Brown, Elmer Guardado-Sánchez, Benjamin M. Spar, Edwin W. Huang, Thomas P. Devereaux, and Waseem S. Bakr. Angle-resolved photoemission spectroscopy of a fermi–hubbard system. *Nature Physics*, 16(1):26–31, Oct 2019.
- [32] A. Bohrdt, D. Greif, E. Demler, M. Knap, and F. Grusdt. Angle-resolved photoemission spectroscopy with quantum gas microscopes. *Phys. Rev. B*, 97:125117, Mar 2018.
- [33] Yuehua Su and Chao Zhang. Coincidence angle-resolved photoemission spectroscopy: Proposal for detection of two-particle correlations. *Phys. Rev. B*, 101:205110, May 2020.
- [34] P. W. Anderson and C. J. Gorter. Chapter i the josephson effect and quantum coherence measurements in superconductors and superfluids. In *Progress in Low Temperature Physics*, volume 5, pages 1–43. Elsevier, 1967.
- [35] J. T. Anderson, R. V. Carlson, and A. M. Goldman. Pair tunneling as a probe of order-parameter fluctuations in superconductors: Zero magnetic field effects. *Journal of Low Temperature Physics*, 8(1):29–46, 1972.
- [36] D. J. Scalapino. Pair tunneling as a probe of fluctuations in superconductors. *Phys. Rev. Lett.*, 24:1052–1055, May 1970.
- [37] Philippe Corboz, T. M. Rice, and Matthias Troyer. Competing states in the t - j model: Uniform d-wave state versus stripe state. *Phys. Rev. Lett.*, 113:046402, Jul 2014.
- [38] Daniel P. Arovas, Erez Berg, Steven A. Kivelson, and Srinivas Raghu. The hubbard model. *Annual Review of Condensed Matter Physics*, 13(1):239–274, 2022.
- [39] A. Bohrdt, E. Demler, and F. Grusdt. Rotational resonances and regge-like trajectories in lightly doped antiferromagnets. *Phys. Rev. Lett.*, 127:197004, Nov 2021.
- [40] A. Bohrdt, E. Demler, and F. Grusdt. Rotational resonances and regge trajectories in lightly doped antiferromagnets. *arxiv:2101.09280*, 2021.
- [41] Annabelle Bohrdt, Eugene Demler, Frank Pollmann, Michael Knap, and Fabian Grusdt. Parton theory of angle-resolved photoemission spectroscopy spectra in antiferromagnetic mott insulators. *Phys. Rev. B*, 102:035139, Jul 2020.
- [42] Thomas Barthel, Ulrich Schollwöck, and Steven R. White. Spectral functions in one-dimensional quantum systems at finite temperature using the density matrix renormalization group. *Phys. Rev. B*, 79:245101, Jun 2009.
- [43] Stefan Meixner, Werner Hanke, Eugene Demler, and Shou-Cheng Zhang. Finite-size studies on the $so(5)$ symmetry of the hubbard model. *Phys. Rev. Lett.*, 79:4902–4905, Dec 1997.

Appendix A: Comparison to string theory

In Figs. 6, 7, and 8, we compare the prediction of the geometric string theory, [15], to the numerically calculated two-hole spectral function in the $t - J_z$ model at $t/J_z = 3$ for s -wave, p -wave, and d -wave pairs, respectively. Due to the finite evolution time in the MPS simulations, the corresponding spectra are broadened. The overall distribution of spectral weight agrees well between string theory and numerical $t - J$ model simulation for all values of m_4 , and moreover, the dispersion of the peaks is in many cases correctly captured. As mentioned in the main text, the MPS simulations on the four-leg cylinder suffers from hybridization between $m_4 = 0$ and $m_4 = 2$, such that remnants of $m_4 = 2$ states are visible in the $m_4 = 0$ spectra and vice versa. The geometric string theory does not suffer from such finite size effects, and no hybridization of different m_4 is possible.

Appendix B: Intuitive picture for flat bands of d -wave pairs

As a nearest neighbor pair with d -wave symmetry moves through the system, the phase structure of the pair can lead to an exact cancellation of the final states. In Fig. 9, such a hopping is depicted for an up/right movement of a pair of distinguishable particles connected by a string. The final configurations are the same for an initial x - and y -configuration of the nearest-neighbor pair, but due to the d -wave symmetry, the signs lead to a cancellation. This intuitive picture is valid in the perturbative regime, $t \ll J_z$, since the pair size is small and the hopping of the pair considered here is a higher order process. Our numerics presented in the main text and semi-analytical calculations presented in [15] indicate that this destructive interference is equally present beyond the perturbative regime $t \geq J_z$.

Appendix C: Experimental detection of pairs

To experimentally probe our predictions in solids, we discuss different possible approaches. The first method is to use coincidence angle-resolved photo-emission spectroscopy (cARPES) [33], which relies on simultaneous measurements of two photo-electrons and provides direct insights into the pair Green’s function. As a main advantage of this approach it directly provides energy and momentum resolution across the entire Brillouin zone. A main disadvantage is that only s -wave pairs can be detected without further complications.

A second method assumes as a starting point an unpaired state of magnetic polarons around their dispersion minimum at momentum $(\pi/2, \pi/2)$. This state can either be assumed to be realized in equilibrium, or a previous ARPES pump pulse can create an initial occupation of magnetic polarons around $(\pi/2, \pi/2)$. Then a probe

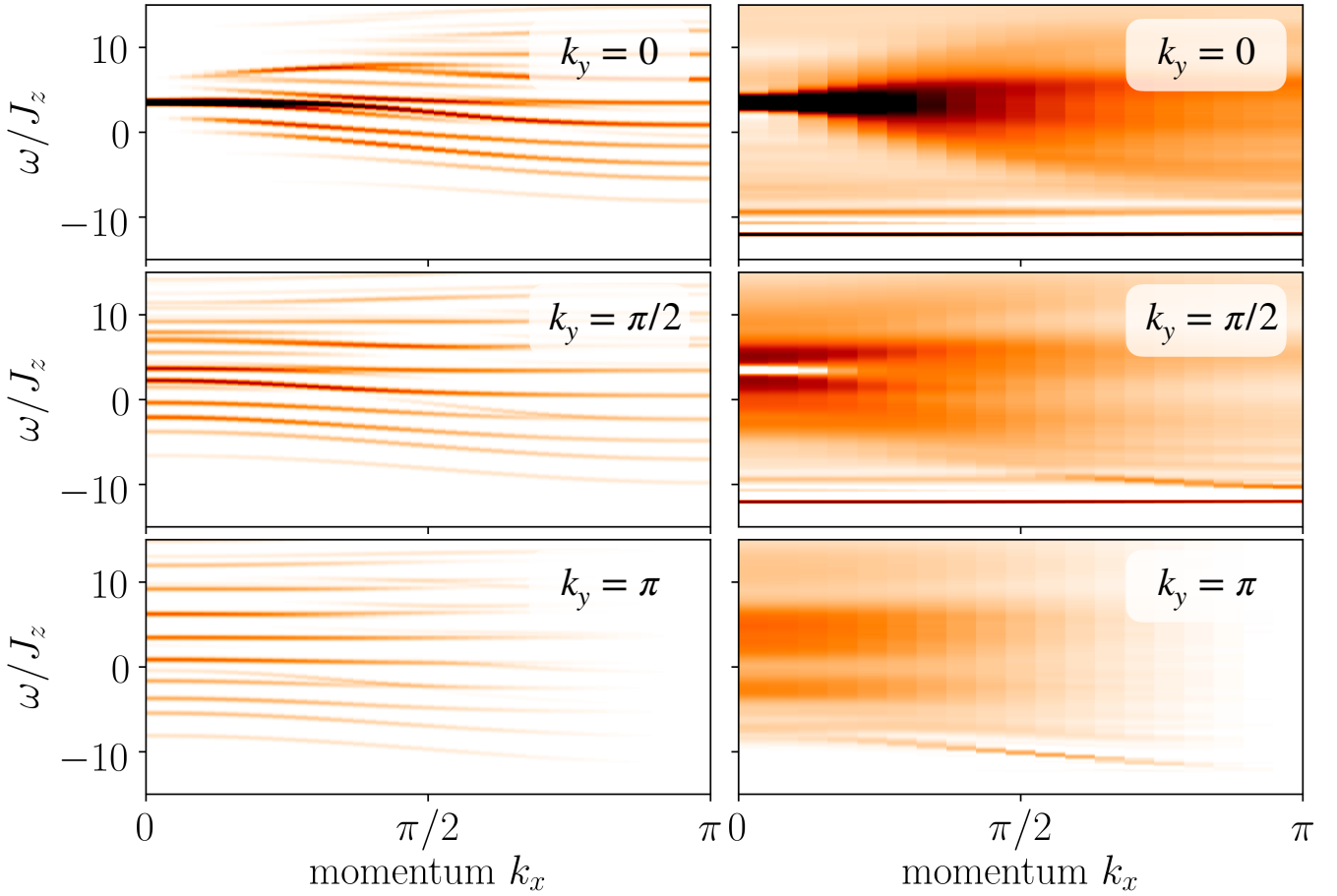


FIG. 6. **Comparison of *s*-wave spectra to geometric string theory prediction**, [15], left, to numerically calculated spectra (right), for the $t - J_z$ model with $t/J = 3$, $\chi = 600$, time evolution up to $T_{max}/J_z = 10$, on a 40×4 cylinder. Top, middle, bottom plots correspond to momentum $k_y = 0, \pi/2, \pi$, respectively.

ARPES pulse is used to create pairs of holes directly from the initial magnetic polarons whose energy and momentum is known. To avoid an undesired signal from newly created magnetic polarons by the second ARPES beam, the ARPES signal without any prior doping can be subtracted. We envision that non-zero angular momentum channels $m_4 \neq 0$ can also be addressed using this method, if the initial magnetic polarons are created in a rotationally excited state [39] using a two-photon scheme involving a driven phonon mode carrying non-zero C_4 angular momentum m_4 [40].

A third approach is based on Anderson-Goldman pair tunneling in a tunnel junction setup [35]: to study the structure of individual pairs in a strongly underdoped quasi-2D material as considered here, we propose to tunnel-couple the latter to a probe-superconductor along z direction. By applying an in-plane magnetic field H_y along y and a voltage V across the junction, Cooper pair tunneling from the physical to the probe layer can be described by an effective Hamiltonian of the form [34, 36]

$$\hat{\mathcal{H}} = -g \int dx dy e^{i(qx - \omega t)} \Delta_p(x, y) \hat{\Delta}_{m_4}^{(s)}(x, y) + \text{h.c.} \quad (\text{C1})$$

Here $\Delta_p(x, y)$ is the order parameter in the probe-superconductor, which is assumed to be well below its critical temperature $T \ll T_c$. By choosing different singlet superconductors as probes, situations with *s*- or *d*-wave pairing symmetry ($m_4 = 0$ or $m_4 = 2$) could be realized. In the physical system this introduces the proximity-coupling term $\hat{\Delta}_{m_4}^{(s)}(x, y)$ introduced previously, with the same pairing symmetry as in the probe. The coupling strength $g \propto t_{sp}^2$ is proportional to the weak tunnel coupling t_{sp} of the junction.

The in-plane momentum q along x , i.e in the plane of the junction and perpendicular to the magnetic field, can be tuned by H_y [36]

$$q = \frac{2eH_y}{\hbar c} (\lambda + d/2) \quad (\text{C2})$$

with λ the magnetic penetration depth of the probe-superconductor and d the thickness of the physical sam-

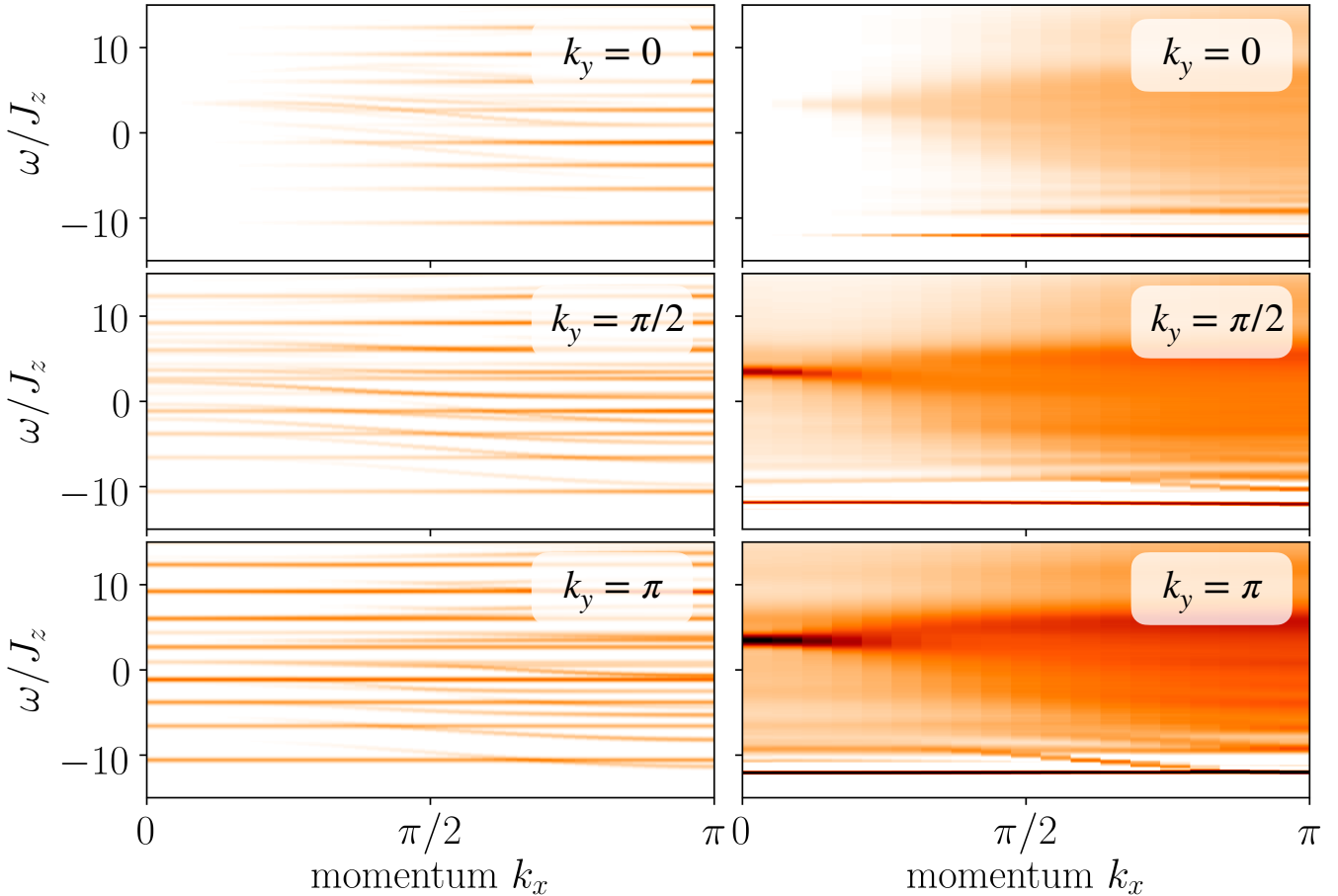


FIG. 7. **Comparison of p -wave spectra to geometric string theory** prediction, [15], left, to numerically calculated spectra (right), for the $t - J_z$ model with $t/J = 3$, $\chi = 600$, time evolution up to $T_{max}/J_z = 10$, on a 40×4 cylinder. Top, middle, bottom plots correspond to momentum $k_y = 0, \pi/2, \pi$, respectively.

ple where the pairs are created. The frequency $\omega = 2eV/\hbar$ is controlled by the voltage across the junction.

In principle this setup allows to measure the frequency and momentum resolved tunnel-current $I(\omega, \mathbf{q})$ across the junction, which is expected to exhibit peaks when (meta-) stable paired states of holes are created in the sample. The positions of these peaks reveal the two-hole spectra we predicted in our article. The main drawback of the tunnel-junction approach is the limited range of momenta $q \ll 1/a$, where a is the lattice constant, that can be accessed by realistic magnetic fields. However, provided enough frequency resolution can be achieved, exploring the small- q regime would be sufficient to measure the effective mass of the hole pairs.

In ultracold atomic systems similar spectroscopic methods can be implemented by tunneling into a second probe system [31, 32]. By considering two-particle hoppings and paired final states, the desired pair Green's function can be measured in such settings. Moreover, by combining them with additional lattice modulations, the angular momentum of the pairs can be modified [40].

Appendix D: MPS simulations

In order to obtain the spectral functions shown in the main text, we follow the same procedure described in detail in [41] and [39]. In the following, we discuss the procedure as well as different convergence checks in more detail.

1. Convergence

We calculate the real-time and -space rotational Green's function based on the singlet pair operator Eq. (3) using time-dependent matrix product states. The time evolution used for the rotational spectra shown in the main text is calculated using the $W^{(II)}$ method [17] with a time step of $dt = 0.02/J$. The resulting real-space and real-time Green's function is shown in Fig. 10 for different bond dimensions χ (increasing opacity corresponds to increasing bond dimension) for two exemplary distances.

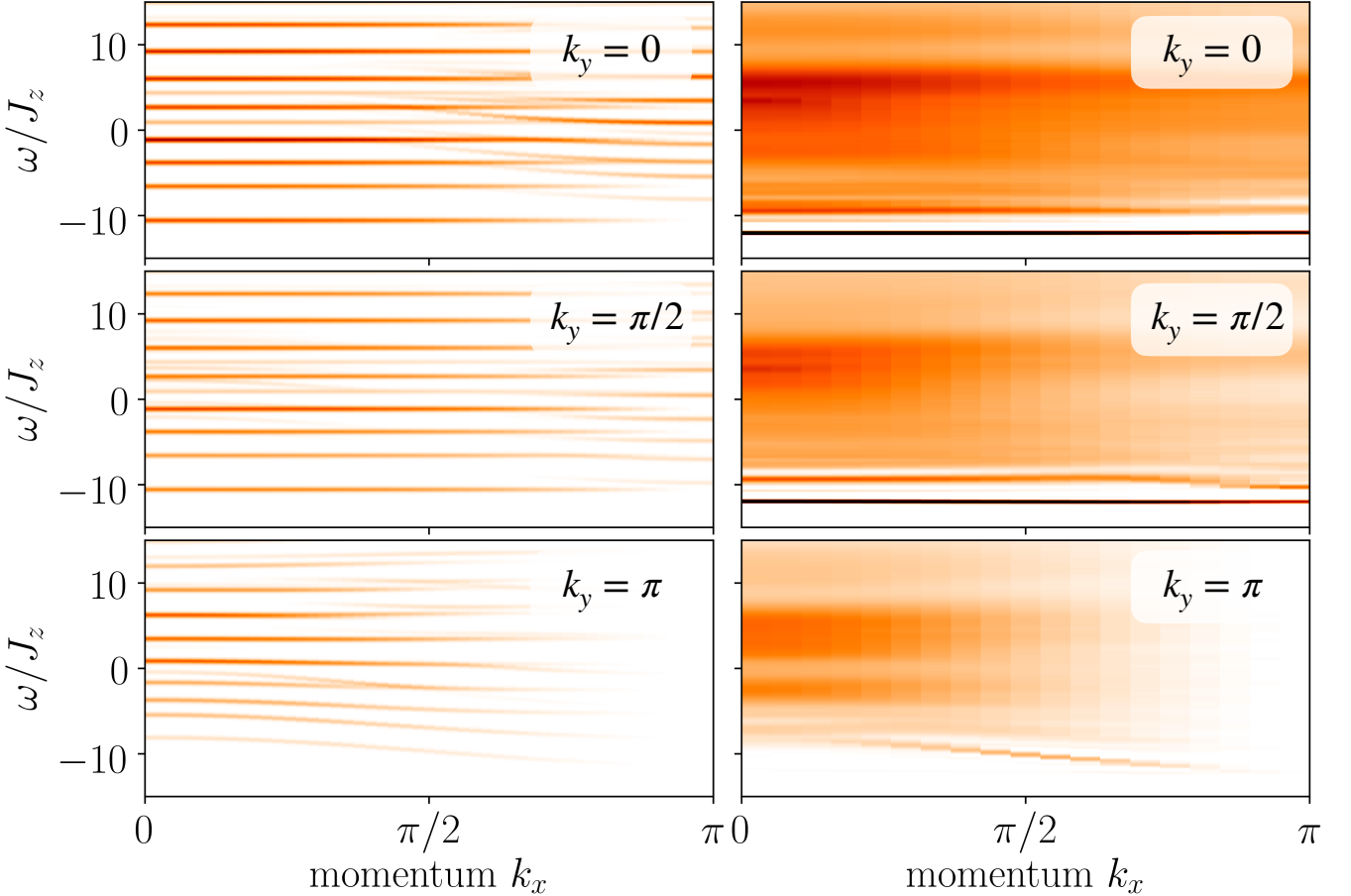


FIG. 8. **Comparison of d -wave spectra to geometric string theory** prediction, [15], left, to numerically calculated spectra (right), for the $t - J_z$ model with $t/J = 3$, $\chi = 600$, time evolution up to $T_{max}/J_z = 10$, on a 40×4 cylinder. Top, middle, bottom plots correspond to momentum $k_y = 0, \pi/2, \pi$, respectively.

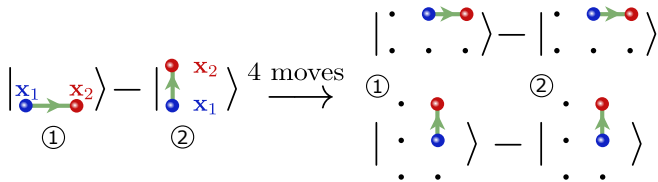


FIG. 9. **Intuitive picture** for the appearance of flat bands for d -wave pairs.

We then perform a Fourier transform to momentum space to obtain $\mathcal{G}_{\text{rot}}^{(m_4)}(\mathbf{k}, t)$, Eq. (5). Subsequently, perform a linear prediction in order to extend our time signal beyond the computationally accessible regime [42]. Finally, the time signal is multiplied by a Gaussian envelope $w(t) = \exp[-0.5(t\sigma_\omega)^2]$, where $\sigma_\omega = \sigma/T_{\max}$. The Fourier transformed signal, i.e. the resulting spectral function, is shown for different choices of the width of the Gaussian envelope in Fig. 11.

As can be seen in Fig. 11, the finite evolution time leads to some artifacts in the Fourier transformed sig-

nal, in particular some negative values of the spectral function. Increasing σ_ω leads to broader peaks, but also suppresses the sharp cutoff from the finite evolution time more effectively, thus reducing the un-physical negative signal.

2. Extraction of peak position

We extract the positions of the peaks shown in Figs. 3 and 4 of the main text by determining the lowest value of ω at which $A(\mathbf{k}, \omega^* - \Delta\omega) < A(\mathbf{k}, \omega^*)$ and $A(\mathbf{k}, \omega^* + \Delta\omega) > A(\mathbf{k}, \omega^*)$, where $\Delta\omega$ is the resolution in frequency space. We set a minimum height of the peak $A(\mathbf{k}, \omega^*) \geq 0.05$ in order to discard artifacts of the Fourier transform.

3. Singlet versus triplet excitations

In Fig. 13, the rotational two-hole spectrum is compared for the case of a singlet excitation, Eq. 4, and a

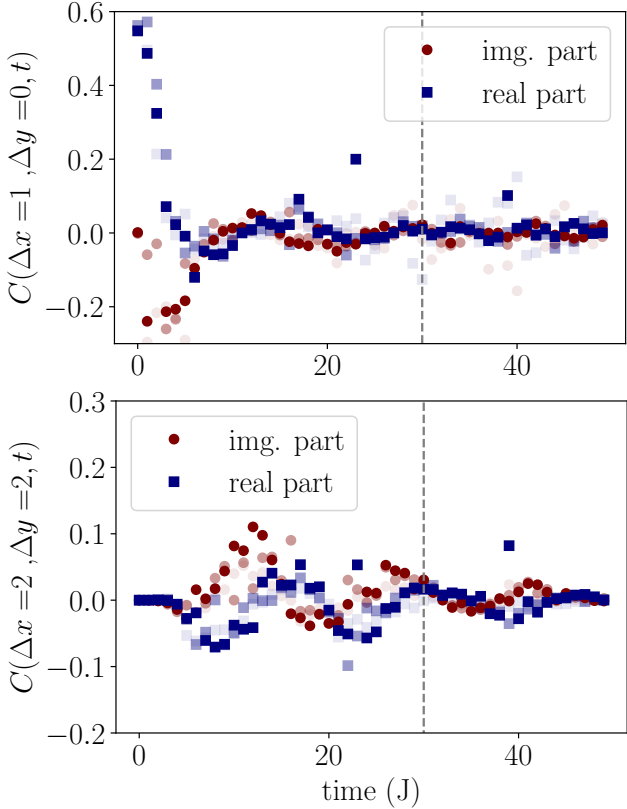


FIG. 10. **Convergence with bond dimension.** Real-space and -time Green's function at exemplary distances Δx , Δy (top and bottom) for bond dimensions $\chi = 600, 1200, 2000$ (increasing opacity) for the $t - J$ model. The rotational spectra shown in the main text and supplementary material are based on the time evolution up to $T_{\max} = 30$ (gray dashed line).

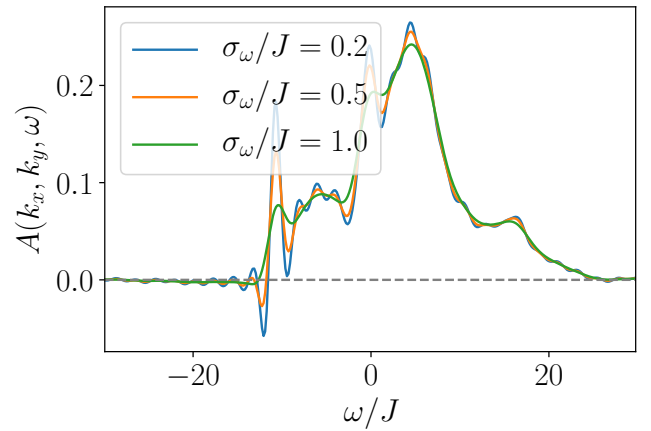


FIG. 11. **Gaussian envelope.** Spectral function at $k_x = \pi/2, k_y = 0$ for different widths σ_ω of the Gaussian envelope for the $t - J$ model with $t/J = 3$, $\chi = 1200$. The rotational spectra shown in the main text and supplementary material are based on the time evolution up to $T_{\max} = 30$ and Gaussian envelope width $\sigma_\omega/J = 0.5$.

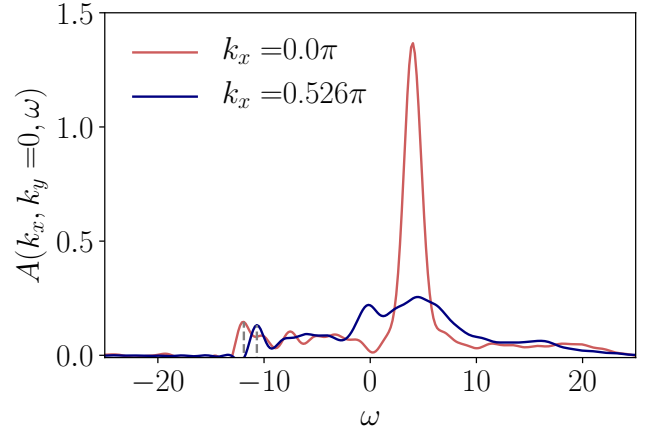


FIG. 12. **Extracting peak positions** from the spectral function, here shown for $k_y = 0$ and k_x as indicated for the $t - J$ model with $t/J = 3$, $\chi = 1200$. The peak positions shown in main text Figs. 3 and 4 correspond to the dashed gray lines in this plot.

triplet excitation, Eq. 9 for the $t - J$ model. As expected, the overall amplitude of the triplet excitation is significantly lower than in the case of a singlet excitation; note the different color scale. Moreover, the lowest energy peak for the triplet excitation is at a higher energy than the corresponding lowest energy peak in the singlet excitation spectrum.

The triplet excitation spectra at momentum $\mathbf{k} = (\pi, \pi)$ is related to the dynamical correlation functions involving $\pi_{s/d}^\dagger$ operators considered in [43]. Consistent with this earlier work on finite size Fermi-Hubbard models, a low energy peak with high spectral weight is visible in the d -wave spectra. In the s -wave case, we observe a low-energy peak with strongly suppressed spectral weight. We argue that this peak appears in the s -wave case due to the hybridization of $m_4 = 0$ and $m_4 = 2$ excitations on the finite width cylinders accessible with time-dependent matrix product states. The majority of spectral weight in the s -wave case is at high energies.

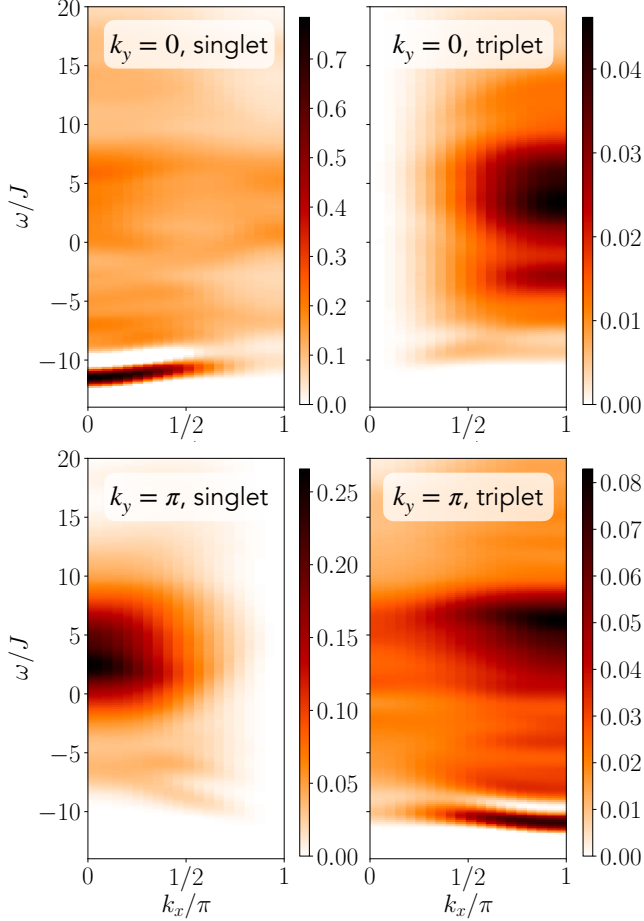


FIG. 13. **Singlet vs triplet excitation.** Rotational two-hole spectra in the $t - J$ model with $t/J = 3$ for $m_4 = 2$ (d -wave) and $k_y = 0$ (top) and $k_y = \pi$ (bottom) for singlet (left) and triplet (right) excitation, obtained from time-dependent matrix product state simulations of the singlet two-hole rotational spectrum.

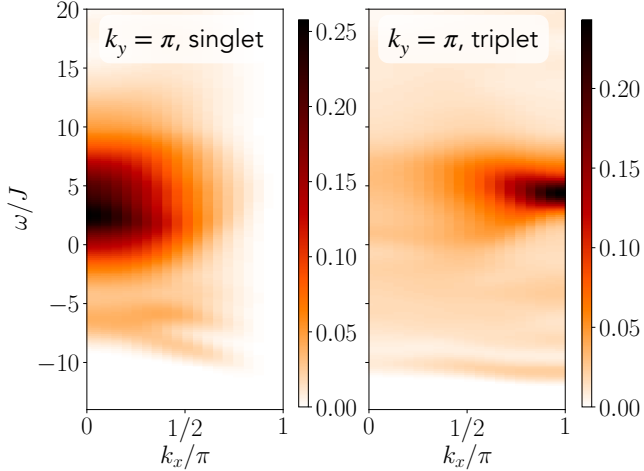


FIG. 14. **Singlet vs triplet excitation.** Rotational two-hole spectra in the $t - J$ model with $t/J = 3$ for $m_4 = 0$ (s -wave) and $k_y = \pi$ for singlet (left) and triplet (right) excitation, obtained from time-dependent matrix product state simulations of the singlet two-hole rotational spectrum.

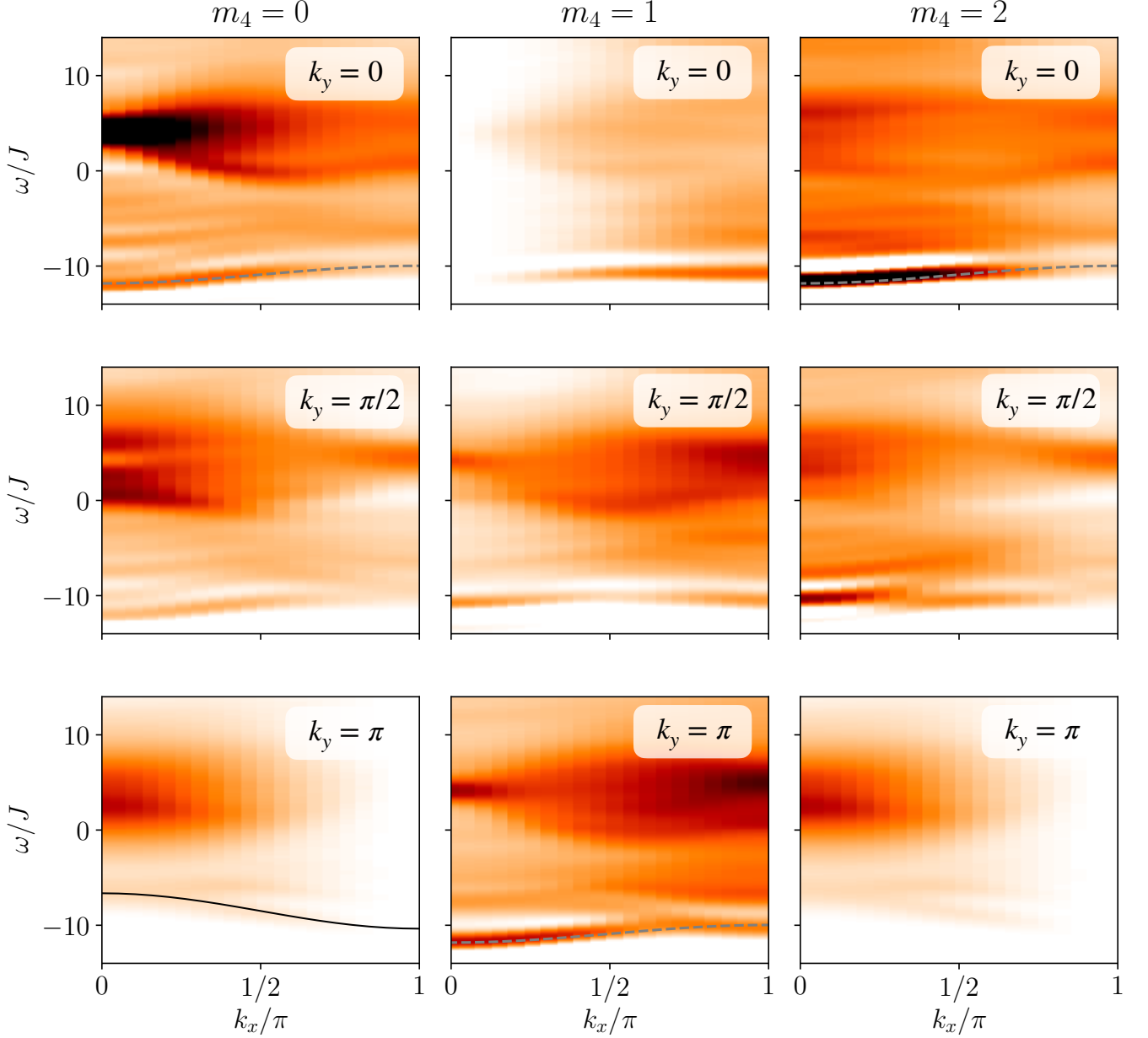


FIG. 15. **Angular momentum dependence** of the rotational two-hole spectra in the $t - J$ model with $t/J = 3$ for $m_4 = 0, 1, 2$ (left, middle, right column) and $k_y = 0, \pi/2, \pi$ (top, middle, bottom row). The colormap corresponds to matrix product state simulations of the singlet two-hole rotational spectrum. The black line corresponds to the cosine fit to the lowest dispersive feature at $k_y = \pi$, see Fig. 3. The gray dashed lines correspond to the cosine fit to the lowest peak at $k_y = 0$, see Fig. 4.